PUBLISHED VERSION

T. Reynolds, A. François, M.R. Henderson, S.J. Nicholls, T.M Monro
Optimization of whispering gallery mode sensor design for applications in biosensing

http://hdl.handle.net/2440/92461

Optimization of whispering gallery mode sensor design for applications in biosensing

T. Reynolds *[a], A. François [a], M.R. Henderson [a], S.J. Nicholls [b], T.M Monro [a, c]

[a] The Institute for Photonics and Advanced Sensing (IPAS) and ARC Centre of Excellence for Nanoscale BioPhotonics (CNBP), University of Adelaide, Adelaide SA 5005, Australia; [b] South Australian Health and Medical Research Institute (SAHMRI), Adelaide SA 5000, Australia; [c] University of South Australia, Adelaide SA 5000, Australia

*email address: tess.reynolds@adelaide.edu.au

ABSTRACT

Whispering gallery modes (WGM) within microsphere cavities have demonstrated the ability to provide label-free, highly sensitive and selective detection down to a single molecule level, emerging as a promising technology for future biosensing applications. Currently however, the majority of biosensing work utilizing WGMs has been conducted in resonators made from either silica or polystyrene while other materials have been largely uninvestigated. This work looks to predict the optimal combinations of material, resonator size and excitation/coupling scheme to provide guidelines to assist in decision making when undertaking refractive index biosensing in a range of situations.

Keywords: Whispering gallery modes, biosensing, optimization, microsphere

INTRODUCTION

Whispering gallery modes (WGM) with in microsphere resonators have become a well established technique for a large range of different biological sensing applications due to their demonstrated ability to conduct highly sensitive [1], selective [2] and label-free detection of molecules and proteins [3-5], extending down to the single molecule level. WGMs arise due to light being trapped along the microsphere's circumference due to total internal reflection along its boundary. As the light circulates within the microsphere, a fraction of the light extend outside of the resonator into the surrounding medium through the evanescent field, allowing changes in the outside environment to be monitored. One interesting properties of WGM resonators is the amount of time the light remains circulating within the resonator and is described by the quality factor (Q). The Q can be characterized in a range of different ways and is most commonly defined in terms of quantities such as loss mechanisms of the resonator (absorption, scattering, radiation) [6], resonance wavelength and linewidth as well as the cavity ring down time [7]. The higher the Q, the narrower the resonance linewidth becomes, allowing smaller shifts in the resonance position to be detected, which is favorable for sensing applications. Previously, the majority of work undertaken in the WGM biosensing field has been conducted in predominately two materials, namely polystyrene [8,9] and silica [10,11]. The silica microspheres used range typically from 50-100μm in diameter and are produced via melting the tip of an optical fibre [12, 13]. After the melting process, the microsphere remains attached to the fibre, allowing it to be easily secured with an optical set up. Light from a tunable laser can then be coupled into the sphere via a number of commonly used methods such as, waveguides [14], coupling prisms [15] and fiber tapers [16]. Using these types of setups, Q factors in silica microspheres have reached as high as $\sim 0.8 \times 10^{10}$ [17]. However, precise alignment is required when using any of these coupling methods, reducing their practicality to be used in some biosensing situations such as for *in-vivo* sensing [18] as any change in the resonance wavelength peak position due to a refractive index change or a binding event that is being studied is indistinguishable from any alteration in the coupling efficiency. This leads to the other commonly used material in polystyrene, as it provides a contrasting method based on fluorescent dye-doped microspheres that allows for remote sensing, albeit at a significantly lower Q. In order to capitalize on the benefits of fluorescent based sensing, new materials need to be investigated to help bridge the gap in sensing performance between the two regimes. One method to begin the investigation, allowing a large number of different resonator materials and sizes to be examined, is through analytical modeling [19,20]. By simulating the WGM spectrum that would be produced, information such as sensitive and Q can be characterized, giving insight into the sensor performance prior to conducting experiments.

THEORETICAL MODEL

For any dielectric microsphere of radius R and refractive index n_1 the whispering gallery mode (WGM) spectrum can be generated by extending on classical Mie Scattering theory, as demonstrated by Chew [20]. Consider an arbitrary distribution of dipoles within a spherical dielectric resonator, of radius R and refractive index n_1, within a medium of refractive index n_2, being excited by an incident plane wave. The resulting total average power radiated from the sphere is given by the sum of the radial and tangential oscillations, as defined in [20], noting that in the original publication [20] the $(2n+1)/3$ term in the summation of Eq. (1) was omitted from the published equation,

$$P = 2H \sum_{n=1}^{\infty} \frac{2n+1}{3} \left(\frac{J_n}{|D_n|^2} + \frac{GK_n}{|D_n'|^2} \right) \tag{1}$$

where,

$$H = \frac{9\varepsilon_1}{4\rho_1^5} \sqrt{\frac{\varepsilon_1 \varepsilon_2 \mu_1}{\mu_2}}, \; G = \frac{\varepsilon_1 \varepsilon_2}{\mu_1 \mu_2},$$

$$K_n = \left(\frac{\rho_1^3}{2} \right) \left[j_n^2(\rho_1) - j_{n+1}(\rho_1) j_{n-1}(\rho_1) \right], \; J_n = K_{n-1} - n\rho_1 j_n^2(\rho_1)$$

$$D_n = \varepsilon_1 j_n(\rho_1) \left[\rho_2 h_n^{(1)}(\rho_2) \right]' - \varepsilon_2 h_n^{(1)}(\rho_2) \left[\rho_1 j_n(\rho_1) \right]', \; D_n' = Dn(\varepsilon_{1,2} \to \mu_{1,2}),$$

$$\rho_{1,2} = k_{1,2} R.$$

The positions of the resonance peaks in the WGM spectra generated using the Chew model have been previously shown to align with those predicted using classical Mie Scattering formulations [21], while recently we have confirmed that the model is also in agreement with computational simulations based on the Finite-Difference Time Domain (FDTD) method [22]. This is useful as the Chew model is significantly less computationally expensive to run compared with FDTD simulations, providing a quicker and simpler alternative to examine spectral information of any resonator (R, n_1) combination. However, FDTD still provides insight extending beyond spectral information including transient phenomena as well as being able to consider other resonator geometries, which is not possible from the Chew model.

RESULTS AND DISCUSSION

Implementing the analytic model described above, the whispering gallery mode spectrum for microspheres with diameters ranging from $D = 1 - 20\mu m$ and refractive indices ranging from $n_1 = 1.45 - 2.0$ immersed in water ($n_2 = 1.3325$) were simulated over the wavelength range 600-615nm, corresponding to the fluorescence region of commonly used organic dyes such as Nile Red [23], and analyzed to predict the sensing performance. The analysis involves the identification of the position and intensity of each peak present in the spectrum, along with passing the individual peaks through fitting routines to calculate the Q while also calculating the refractive index sensitivity by monitoring the change in the spectrum as the surrounding refractive index was varied. Finally, by combing the sensitivity and Q, the minimum achievable detection limit is determined for each resonator.

Refractive index sensitivity

The refractive index sensitivity is calculated by considering the shift in the resonant wavelength position due to a change in the surrounding refractive index.

$$S = \frac{\Delta \lambda}{\Delta n} \tag{2}$$

Although the sensitivity can be calculated using simpler analytical models that just produce the peak positions, utilizing the Chew model to generate the entire WGM spectrum allows not only the peak positions to be monitored but also other information such as how the Q changes during this process, as demonstrated in Fig 1(A).
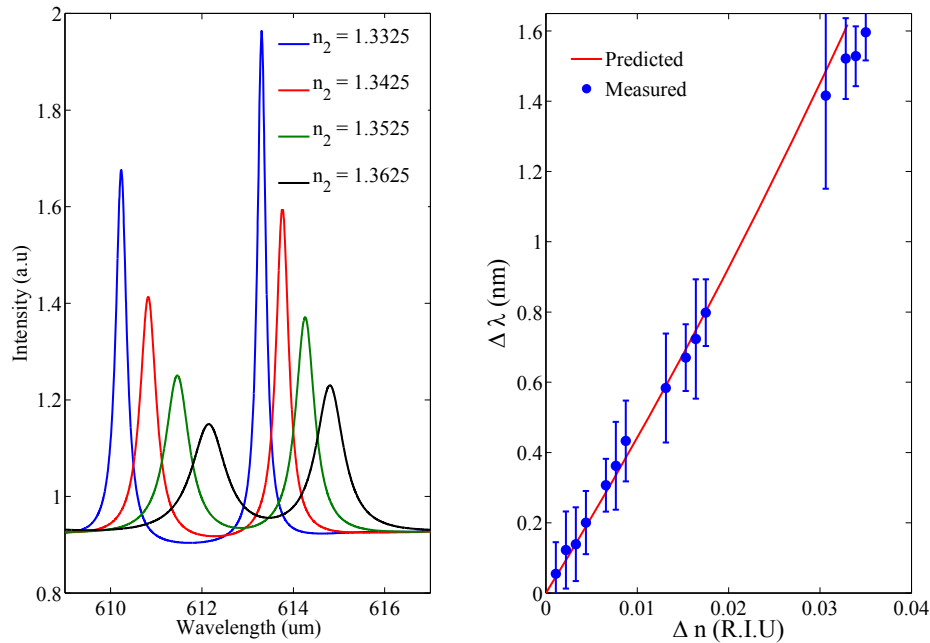

Fig. 1. (A) Change in position of the resonance peaks for a 6μm radius polystyrene sphere (n_1 = 1.59) initially in water (n_2 = 1.3325) for incremental increases in the surrounding refractive index n_2 by 0.01 R.I.U. (B) Comparison of the predicted sensitivity from the model (red line) to the measured sensitivity of a $R\sim5$μm polystyrene sphere in water.

To evaluate the sensitivity across the parameter space, firstly the initial spectrum for the resonator (R, n_1) immersed in water (n_2 = 1.3325) was generated and then new spectra are generated by increasing the value of n_2 (step size 0.005 R.I.U) until the surrounding refractive index has increased by 0.01 R.I.U, monitoring the shift in the position of the resonance peaks at each step. The predicted sensitivity is compared to the measured sensitivity for a polystyrene sphere in water with $R \sim 5$μm and the result is shown in Fig 1(B). Good agreement is seen between the model and experimental data. As expected, the shift in the position of the resonance peaks $\Delta\lambda$ displays a linear response to the changes in n_2 over the range of Δn considered, even as extends Δn to values that are higher than that typically observed in refractive index sensing experimentally. Non-linear responses in $\Delta\lambda$ were observed as Δn became greater than 0.04 R.I.U.

Figure 2 displays the refractive index sensitivity as a function of radius and refractive index of the resonators considered across the entire parameter space. The solid black line seen running across the figure defines the boundary below which no peaks would be resolvable above the background fluorescence and so are not considered in the analysis. This arises because the spectra being produced from the Chew model represents the total averaged power radiating from the resonator, which is normalized to the bulk values in the surrounding medium [reference], implying that in order to observed a peak the peak height must be greater than 1. The sensitivity map shows that, as expected, for a given sphere radius R, the sensitivity decreases with increasing sphere refractive index, as the increasing refractive index contrast results in the light becoming more tightly confined within the resonator. The region corresponding to the highest sensitivity is located just above the boundary defined by the peak heights of the spectrum, showing that the higher the refractive index, the smaller the sphere can be to get the same level of sensitivity.
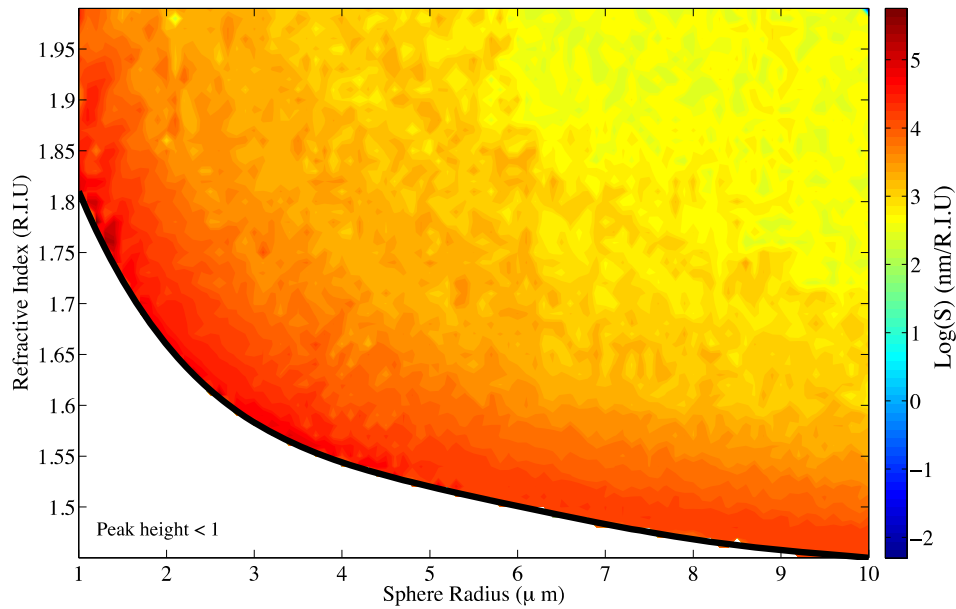
Fig.2. Contour plot of the sensitivity derived using the analytical Chew model for spherical resonators over the parameter space ranging from $a = 1\mu m - 10\mu m$ and refractive index range from $n_1 = 1.45 - 2.0$ within the wavelength range of 600-615nm. Note the scale is logarithmic.

Quality factor

Using the Chew model to generate a WGM spectrum, the quality factor of the cavity, Q_c, can be calculated using the resonance wavelength λ and linewidth $\Delta\lambda$ via,

$$Q_c = \frac{\lambda}{\Delta\lambda}.$$ (3)

Over the entire parameter space, from the generated WGM spectrum, Q_C was evaluated using Eq. (3) for each peak that appeared in the spectrum, with the peak corresponding to the highest value being recorded. Note that this peak is not necessarily the same peak that provides the highest sensitivity calculated above. The contour plot of Q_C calculated over the parameter space is displayed in Fig. 3, including a limit placed on the achievable Q corresponding to the finite resolution of the spectrometer if the spectrum were being observed experimentally. With no consideration of such a limit, the Q would continue to increase exponentially, predicting Q values orders of magnitude grater than what is observed experimentally. Currently in our experimental set-up, detailed elsewhere [18,24], the resolution of the spectrometer is limited to 4 picometers. Once again, the solid black line seen on the figure represents the boundary below which the peaks would not be resolvable above the background fluorescence.

The model however, assumes a perfect dielectric sphere with no loss mechanisms; therefore to provide a more realistic value comparable with experimental observations, material, scattering (due to surface imperfections) and radiation losses also need to be considered. Expressing Q in terms of these loss mechanisms, where Q_m, is the material loss, Q_s is the scattering loss due to surface imperfections, Q_r is the radiation loss and Q_c is as above,

$$\frac{1}{Q} = \frac{1}{Q_m} + \frac{1}{Q_s} + \frac{1}{Q_r} + \frac{1}{Q_c}$$ (4)
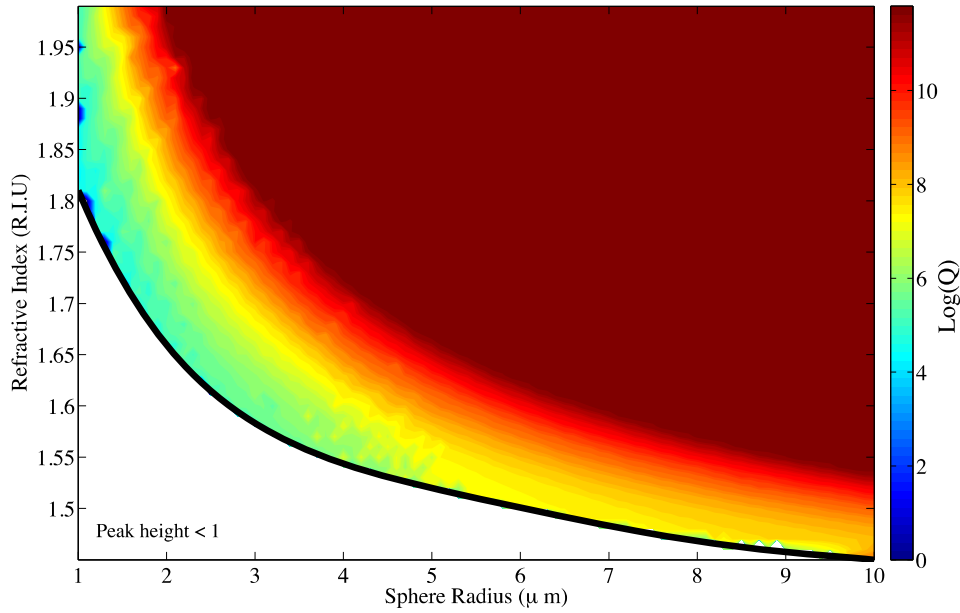
Fig. 3. The quality factor, Q_C, derived using the analytical Chew model for spherical resonators, including the limit placed on the observable Q of fluorescence based WGM due to the finite resolution of the spectrometer used, over the parameter space ranging from $a = 1\mu m - 20\mu m$ and refractive index range from $n_1 = 1.45 - 2.0$ within the wavelength range of 600-615nm. Note the logarithmic scale.

Radiation loss is significant only in situations where total internal reflection can no longer trap light within the resonator, i.e. when the resonators with small radii or a low refractive index contrast. The maximum value of Q_r has been demonstrated to increase exponentially with resonator size, for example, for a silica sphere in water if the ratio $R/\lambda > 15$ then $Q_r > 10^{11}$ [17]. For materials such as polystyrene and glasses with higher refractive indices [25], this limit is even higher, indicating that the contribution to Q is negligible.

Scattering losses can be calculated by modeling the surface roughness as a function of changing dielectric constant and has been used to determine upper limits on the Q of large silica spheres [26]. An expression for the Q limitation due to surface scattering is given by,

$$Q_s = \frac{K_{TE}}{1+K_{TE}} \frac{3\lambda^3 a}{8n_1\pi^2 B^2\sigma^2} \tag{5}$$

where K_{TE} is defined as the ratio of complete scattered power over the power scatter into the angles satisfying angular cutoff conditions as defined elsewhere [26], B is the length and σ is the variance of the surface roughness. As a preliminary test, Q_S was calculated based on the parameters that describe the surface of polystyrene, typically corresponding to a roughness of 15nm or greater [27]. The result produced similar values as that of Q_c, indicating that its contribution to Q through Eq. (3) is insignificant. Adjusting the value of B and σ and monitoring the value of Q_s it was only when the surface roughness was increased towards 50nm that the Qs value had an effect on Q. This level of surface roughness is unlikely to be seen in any of the materials considered.

For the material absorption, the loss can be characterized by considering the absorption of light by both the surrounding medium and the resonator using an absorption decay constant, α_m, as,

$$Q_m = \frac{2\pi n_1}{\lambda \alpha_m} \tag{6}$$

Over the wavelength range considered, an assumption is made that the absorption displayed by the resonators is the same as that of polystyrene and it has previously been shown that the upper limit Q_m is at least an order of magnitude larger than the Q observed experimentally for polystyrene [28, 29], making its contribution to Q negligible.

Despite the consideration of the three loss mechanisms, there remains a noticeable difference in the measured and predicted Q values (Q ~ 1000 [30] measured and Q ~ 2×10^5 predicted for a 15µm polystyrene sphere in water), as their individual contributions are not noticeable. This difference is though to be a result of one of the assumptions made in deriving the Chew model, namely that the resonator being considered is a perfect dielectric sphere. In reality, the microsphere will not be perfect spherical, and even small deformations in the resonator shape away from a perfect sphere would result in a decrease in the Q.

Consider for example the spectra of three spheres with radii 4.995µm, 5.00µm and 5.005µm, Fig 4(A). Even a small difference of 0.5nm in the radius results in a distinguishable change in the position of the resonance peaks. In each case, the spheres are still assumed to be perfectly spherical and so each of the three spectra show peaks with very similar intensities. If, however, the resonator being considered is not perfectly spherical, i.e. elongated along one axis, then the light being coupled in with experience a range of difference radii, assuming that any deformations are small enough as so the resonator can still sustain WGMs. The final WGM spectrum observed will then be a combination of all the resonance peaks corresponding to each of the radii, resulting in a broadening in the peak. An example of this is shown in Fig 4(B) where a deviation of +/- 0.5nm in the radius of a 5µm polystyrene sphere was considered.
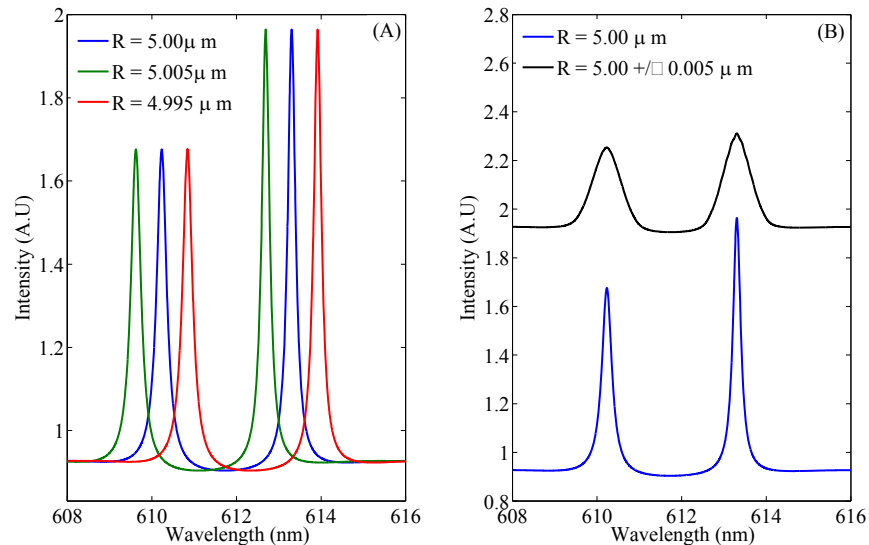

Figure 4. Demonstration on the effect of deformation of the sphere on the Q. (A) WGM spectra of a polystyrene sphere of radius $R = 5$ um (blue line), $R = 5.005$ um (Red) and $R = 4.995$ um (Green) showing the noticeable change in position of the resonance peaks due to a small change in the sphere radius. (B) Assuming the sphere is not deformed too much, the majority of the light will still see the original radius and the other radii will only see a fraction of the light, resulting in a broadening of the peak (black line) from the original perfectly spherical sphere (blue line).

Therefore, over this wavelength range and materials being considered, it is reasonable to conclude that asphericity in the resonator shape is responsible for the large differences between the predicted and measured Q values. This effect is planned for further future investigation.

Detection Limit

The sensitivity and Q provide insight into the performance of the resonator, but for biological sensing applications, the detection limit of the sensor is the key parameter as it determines the smallest viruses, proteins and change in

environmental refractive index that can be measured. An expression for the detection limit can be found by considering the smallest change in the refractive index that can be measured and how it is related to the minimum line with of the resonances (from Q), so through combining Eq. 2 and Eq. 6,

$$\sigma_{LOD} \propto \frac{1}{QS} \qquad (7)$$

In practice however, further considerations [5] for the proteins or molecules being sensed such as molecular weight, excess polarizability, wavelength being utilized along with the fact that only a fraction of the shift in the resonance wavelength position can be observed are to be added as required. The detection limit using Q_C and S calculated over the parameter space is displayed in Fig. 5. As in the maps above, the solid black line running across the figure represents the boundary below which the peaks would not be observable above the background fluorescence. The dotted black line that has been placed on the figure represents the region that corresponds to the minimum detection limit, i.e. where the combination of Q_c and S is maximized. This line correlates with the limit on the Q enforced due to the finite resolution of the spectrometer indicating that for fluorescence based WGM refractive index sensing over this parameter space, the resolution of the spectrometer limits the performance of the resonator. This is expected for this parameter space, as the loss contributions from scattering and absorption are negligible, allowing the Q to continue to increase until it hits the imposed limit. For different parameter spaces, such as at higher wavelengths and larger sphere sizes, this may not be the case with contributions from scattering and absorption losses playing a larger role, shifting the location of the minimum detection limit, and the ideal resonator size and material combination.
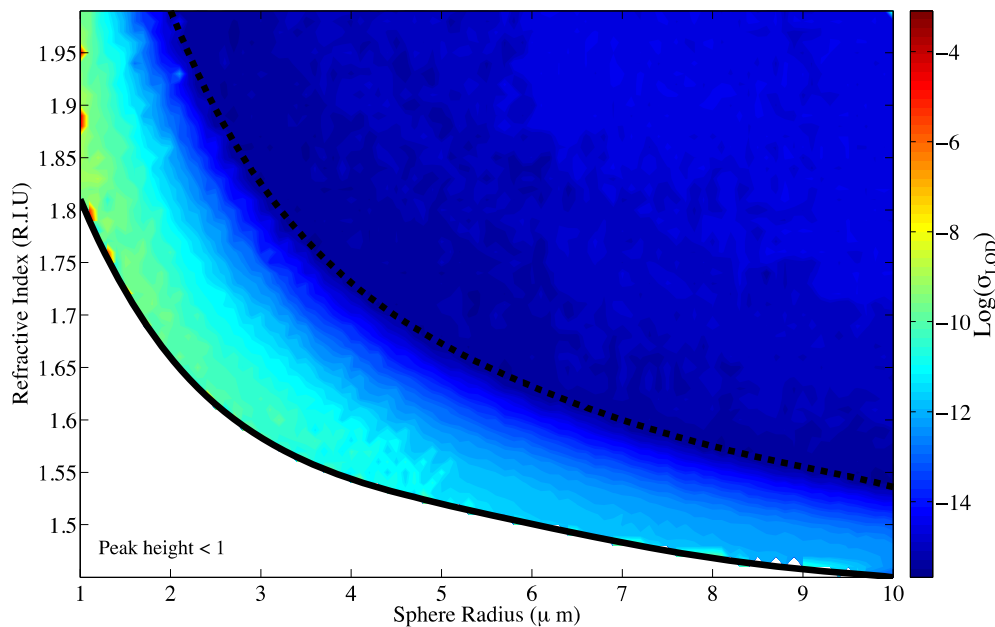

Fig. 5. Detection limit σ_{LOD} mapped over the parameter space $a = 1\mu m – 20\mu m$ and refractive index $n_1 = 1.45 – 2.0$ within the wavelength range 600-615nm. The dotted line represents the minimum value of the detection limit (i.e. where the product QS is maximized). Note the logarithmic scale.

CONCLUSION

By using an analytical model to generate the WGM spectrum of any size and material spherical microresonator, this work demonstrates how the spectral information can be used to predict sensing performance of fluorescence based WGM refractive index sensors. The predicted refractive index sensitivity is shown to have good agreement with measured sensitivity, displaying the expected linear response in the resonance peak position to changes in the surrounding refractive index. The predicted Q however displayed an overestimate of the achievable Q, with the difference being

identified as a result of the model assuming the resonator to be perfectly spherical and in reality small deviations in the resonators shape naturally occur. Taking into about such deviations, the resulting broadening and reduction in intensity of the resonance peaks aligned with what is expected experimentally. Combining the two parameters, sensitivity and Q, a figure of merit for the detection limit was derived whereby additional specific information related to the application of interest can be simply added in where needed, providing a versatile tool. A demonstration of the models potential was provided, looking at fluorescence based WGM refractive index sensing in polymer based materials over a common used wavelength range (600-615nm). It was shown that for this parameter set, the resolution of the spectrometer was the limiting factor on the performance of the sensor. Different parameter sets, i.e. other wavelength ranges, higher refractive indices and larger resonators, the contributions from all the loss mechanisms will be different as so the optimal combinations of size and material will change. Overall, this model provides a relatively easy method for the generation and analysis of the WGM spectrum for any combination of resonator size and material over a given wavelength range, and serves as an initial step in the process of selecting a resonator to be used for biosensing application.

ACKNOWLEDGMENTS

REFERENCES

[1]   Arnold, S., Khoshsima, M., Teraoka, I., Holler, S. and Vollmer, F., "Shift of whispering gallery mode in microsphere by protein absorption," Optics Letters **28**, 272 (2003).

[2]   Vollmer, F., Arnold, S., Braun, D., Teraoka, I., and Lichaber, A., "Multiplexed DNA quantified by spectroscopic shift of two microsphere cavities," Biophysical Journal **85**, 1974-1979 (2003).

[3]   Basske, M.D., Foreman, M.R. and Vollmer, F., "Single-molecule nuclei acid interactions monitored on a label-free microcavity biosensor platform," Nature Nanotechnology **9**, 933-939 (2014).

[4]   Armani, A.M., Kulkarni, R.P., Fraser, S.E., Flagan, R.C. and Vahala, K.J., "Label-free single molecule detection with optical microcavities," Science **317**, 783-787 (2007).

[5]   Vollmer, F. and Arnold, S., "Whispering gallery mode biosensing: label-free detection down to single molecules," Nature Methods **5,** 591 (2008).

[6]   Vernooy, D.W., Ilchenko, V.S., Mabuchi, H., Streed, E.W., and Kinble, H.J., "High-Q measurements of fused-silica microspheres in the near infrared," Optics Letters **23,** 247-249 (1998).

[7]   Cheema, M.I., Mehrabani, S., Hayat, A.A., Peter, Y., Armani, A.M. and Kirk, A.G., "Simultaneous measurements of quality factor and wavelength shift by phase shift microcavity ring down spectroscopy," Optics Express **20**, 9090-9098 (2012).

[8]   Himmelhaus, M., Krishnamoorthy, S. and François, A., "Optical sensors based on whispering gallery modes in fluorescent microbeads: response to specific interactions," Sensors **10**, 6257-6274 (2010).

[9]   Weller, A., Liu, F.C., Dahint, R., and Himmelhaus, M., "Whispering gallery mode biosensor in the low-Q limit," Applied Physics B **90**, 561-567 (2008).

[10]   Wilson, K.A., Finch, C.A., Anderson, P., Vollmer, F., and Hickeman, J.J., "Whispering gallery mode biosensor quantification of fibronection absorption kinetics onto alkysilane monolayers and interpretation of resultant cellular response," Biomaterials **33**, 225-236 (2012).

[11]   Ren, H.C., Vollmer, F., Arnold, S., and Libchaber, A., "High Q microsphere biosensor – analysis for adsorption of rodlike bacteria," Optics Express **15**, 17410-17423 (2007).

[12]   Hanumegowda, N.M., Stica, C.J., Patel, B.C., White, I., and Fan, X.D., "Refractometric sensors based on microsphere resonators," Applied Physics Letters **87,** 201107 (2005).

[13]   Arnold, S., Keng, D., Shopova, I., Holler, S., Zurawsky, W., and Vollmer, F., "Whispering gallery mode carousel – a photonics mechanism for enhanced nanoparticle detection in biosensing," Optics Express **17,** 6230-6238 (2009).

[14]   Ksendzov, A., and Lin, Y., "Integrated optics ring-resonator sensors for protein detection," Optics Letters **30,** 3344-3346 (2005).

[15]   Gorodetsky, M.L. and Ilchenko, V.S., "Optical microsphere resonators: optimal coupling to high-Q whispering gallery modes," Journal of Optics Soceity of America B **16**, 147-154 (1999).

[16]   Armani, D.K., Kippenberg, T.J., Spilane, S.M., and Vahala, K.J., "Ultra-high-Q toroid microcavity on a chip," Nature **421**, 925-928 (2003).

[17]   Gorodetsky, M.L, Savchenkov, A.A. and Ilchenko, V.S., "Ultimate Q of optical microsphere resonators," Optics Letters **21**, 7 (1996).

[18]   François, A., Reynolds, T. and Monro, T.M., "A fiber-tip label free biological sensing platform: a practical approach toward *in-vivo* sensing," Sensors **15**, 1168-1181 (2015)

[19]   Chew, H., "Transition rates of atoms near spherical surfaces," The Journal of Chemical Physics **87**, 1355-1360 (1987).

[20]   Chew, H., "Radiation and lifetimes of atoms inside dielectric particles," Physical Review A **38**, 7 (1988).

[21]   Bohren, C.F., and Huffman, D.R., "Absorption and scattering by a sphere," Wiley-VCH, Verlag GmbH, 82-129 2007.

[22]   Hall, J.M.M., Afshar, S.V., Henderson, M.R., François, A., Reynolds. T., Riesen, N., and Monro, T.M., "Method for predicting whispering gallery mode spectra of active spherical microresonators," arXiv:1410.8606 (2015)

[23]   Greenspan, P., Mayer, E.P. and Fowler, S.D., "Nile Red: A selective fluorescent stain for intracellular lipid droplets," The Journal of Cell Biology **100,** 965-973 (1985).

[24]   François, A., Rowland, K.J., and Monro, T.M., "Highly efficient excitation and detection of whispering gallery modes in dye doped microspehres using a microstructured optical fibre," Applied Physics Letters **99,** 14111 (2011).

[25]   Ruan, Y., Boyd, K., Ji, H., François, A., Ebendorff-Heidepriem, H., Munch, J. and Monro, T.M., "Tellurite microsphere for nanoparticle sensing and novel light sources," Optics Express **22,** 11996 (2014).

[26]   Gorodetsky, M.L., and Prymikov, A.D., "Rayleigh scattering in high-Q microspheres," Optical Society of America B **17,** 6 (2000).

[27]   Zang, J., Xue, L. and Han, Y., "Fabrication gradient surfaces by changing polystyrene microsphere topography," Langmuir **21,** 508 (2005).

[28]   Armani, A.M., Armani, D.K., Min, B., Vahala, K.J. and pillane, S.M., "Ultra-high-Q microcavity operation in H20 and H20," Applied Physics Letters **87,** 15118 (2005).

[29]   Ta, V.D., Chen, R., Ma, L., Ying, L.J. and Sun, H.D., "Whispering gallery mode microlasers and refractive index sensing based on single polymer fibers," Laser Photonics Review **7,** 133-139 (2013)

[30]   François, A., Rowland, K.J., Afshar, S.V., Henderson, M.R., and Monro, T.M., "Enhancing the radiation efficiency of dye doped whispering gallery mode microresonators," Optics Express **21,** 22566-22577 (2013).